Springer

KSME

Journal of Mechanical Science and Technology 24 (2) (2010) 481~487
www.springerlink.com/content/1738-494x
DOI 10.1007/s12206-009-1209-3

Assessment of the high-temperature crack behavior for a 316L stainless steel structure with defects †

Hyeong-Yeon Lee*, Gyeong-Hoi Koo and Jae-Han Lee

Mechanical Engineering Division, Korea Atomic Energy Research Institute, Deadukdaero 1045, Yuseong-gu, Daejeon 305-353, Korea

(Manuscript Received February 26, 2009; Revised September 13, 2009; Accepted October 14, 2009)

Abstract

An assessment of creep-fatigue crack initiation and growth for a 316L stainless steel structure has been carried out according to the current (2007 edition) and previous (2002 edition) versions of the French RCC-MR A16 procedure. Some significant changes have been made in terms of the formulae and material properties, which may cause big differences in the assessment. In this study, the changes in the A16 guide have been quantified for a 316L austenitic stainless steel structure, and the assessment results were compared with those of the observed images from a structural test for a welded component.

Keywords: Creep-fatigue; Crack initiation; Crack growth; 316L stainless steel; Defect

1. Introduction

The structural integrity of a high-temperature component such as a liquid metal reactor (LMR) similar to KALIMER [1], when subjected to thermal cycles at a creep regime, is usually limited by the accumulation of creep-fatigue damage or the creep-fatigue crack growth behavior. The high-temperature design codes, ASME-NH [2], RCC-MR [3], and DDS [4], provide design guidelines for a defect-free body, while the RCC-MR A16 [5], R5 [6], BS7910 [7], API 579 [8], and FITNET [9] provide assessment procedures for a creep-fatigue crack behavior. Among these procedures, the A16 and the R5 provide the most concrete procedures. In the R5 procedure, the material properties are classified as proprietary; while in the A16 guide, A3 [10] provides the material properties necessary for the assessment or design evaluation.

The current version of the A16 guide is the 2007 edition, which has been revised from the previous 2002 edition. The English version of the 2007 edition was published in 2008. Some significant changes have been made in creep-fatigue crack assessment rules in the 2007 edition of the A16 guide, including crack growth formulae of fatigue crack growth (FCG) and creep crack growth (CCG). These changes in the crack growth formulae can make a significant difference in the assessment result. It should also be noted that the RCC-MR material properties, A3, which is used in the evaluation of design or assessment, have been modified. However, no studies on quantifying the changes of the fracture parameter formulae and material properties have yet been carried out. In this study, the changes of the crack growth formulae (A16) and material properties (A3) such as the creep rupture strength and fatigue strength data have been quantified using the two editions.

In a previous study, the assessment of a creep-fatigue crack initiation (C-F CI) and growth (C-F CG) for 316L stainless steel-welded cylinder according to the A16 guide and a comparison of the results with those of the structural tests were carried out and A16 was shown to be reasonably conservative [11, 12].

The A16 guide provides assessment procedures for a C-F CI and C-F CG for an austenitic stainless steel but it does not provide procedures for Mod.9Cr-1Mo steel, which tends to be increasingly adopted in the next generation nuclear plants operating at a creep regime as well as in thermal power plants. Research on developing the assessment procedures on creep-fatigue crack behavior for Mod.9Cr-1Mo steel are underway [13-17].

2. Assessment of creep-fatigue crack behavior

2.1 Finite element modeling

The structural specimen in Fig. 1(a), representing an Intermediate Heat eXchanger (IHX) support structure of a liquid metal reactor [1], has been selected as the target model of the

† This paper was recommended for publication in revised form by Associate Editor Chongdu Cho

*Corresponding author. Tel.: +82 42 868 2956, Fax.: +82 42 861 7697
E-mail address: hylee@kaeri.re.kr

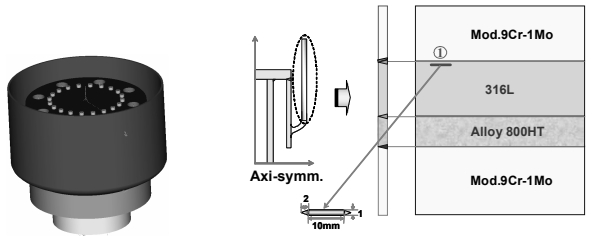

(a) Solid model (b) A development figure of the model

Fig. 1. Structural model of IHX support structure.

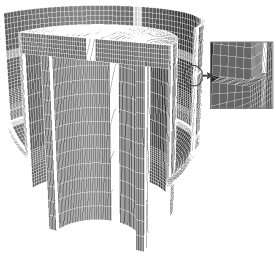

Fig. 2. Finite element model of the 3-D model.

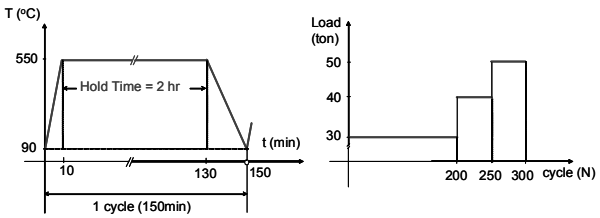

(a) Thermal load (b) Mechanical load

Fig. 3. Load conditions.

present study. The model has a 500 mm diameter, a 440 mm height, and a 6.3 mm thickness. It is made of Mod.9Cr-Mo steel (ASME Grade 91), 316L stainless steel, and Alloy 800HT, as shown in Fig. 1(b).

The three-dimensional (3-D) half-symmetric ABAQUS [18] model was used for the evaluation of the creep-fatigue crack behavior, and an artificial defect was modeled (Fig. 2). As a boundary condition, the bottom surface was fixed rigidly.

The specimen in Fig. 1 was subjected to a thermal cycling with a steady mechanical load. The 316L part of the specimen was heated to 550° C with a tensile hold time of 2 h, as shown in Fig. 3(a). One creep-fatigue load cycle lasted approximately 2.5 h.

The mechanical loads were applied in three steps: 294KN (30 metric tons) inducing a nominal stress of 29.9 MPa at the outer shell for the first 200 load cycles, 40 tons (inducing 39.8MPa) for the next 50 cycles, and finally 50 tons (inducing 49.8 MPa) for the next 50 load cycles, as shown in Fig. 3(b). A total of 300 creep-fatigue load cycles was applied.

2.2 Assessment of the creep-fatigue crack initiation

In the French high temperature design guideline of the RCC-MR code [3, 5], geometrical discontinuities or defects

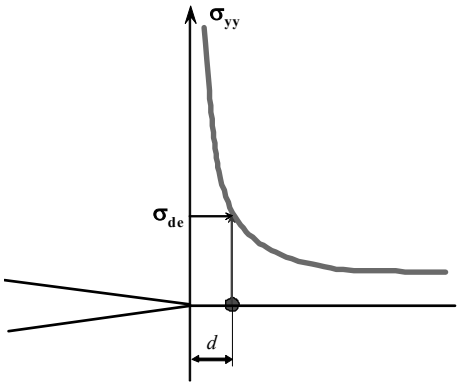

Fig. 4. Sigma-d (σ_{de}) stress at location '*d*' and its calculation using FE analysis.

are assimilated with cracks for a creep-fatigue estimation based on a simplified elastic analysis. The sigma-d (σ_d) approach has been provided in the A16 guide for estimation of an initiation period for a fatigue crack growth from notch or crack-like defects. This method is based on a stress value at a distance, d=50 μm, for austenitic stainless steel ahead of notch or crack-like defects, as shown in Fig. 4.

In order to evaluate a C-F CI, the total strain range according to the A16, ($\overline{\Delta\varepsilon}$) should first be determined. The total strain range is obtained by summing up the strain ranges due to the elasto-plasticity and the creep, as shown in Eq. (1) [5].

$$\overline{\Delta\varepsilon} = \overline{\Delta\varepsilon}_{el+pl} + \overline{\Delta\varepsilon}_{cr} \tag{1}$$

Here, the elastic-plastic strain range ($\overline{\Delta\varepsilon}_{el+pl}$) is determined by adding the four strain terms. The creep strain range ($\overline{\Delta\varepsilon}_{cr}$) is determined for a given hold time during one creep-fatigue load cycle. The creep strain formula for a 316L stainless steel at a primary creep employs the Bailey-Norton form of Eq. (2) over the temperature range of 425<T (° C) ≤600 [10].

$$\varepsilon_{cr} = c_1 t^{c_2} \sigma^{n_1} \tag{2}$$

where $c_1 = 1.155\times10^{-9}$, $c_2 = 0.4537$, $n_1 = 3.153$.

The calculation results of the total strain range ($\overline{\Delta\varepsilon}$) according to the A16 procedure were 0.445%, 0.523%, and 0.622% for the mechanical load cases of 30, 40, and 50 tons, respectively.

It should be noted that the material properties related to the above assessment (A3), including the creep rupture stress and fatigue strength data, have been changed. It is interesting to see that for long-term creep zone, the creep rupture strength in the 2007 edition has been decreased from that of the previous version, whereas the fatigue strength has been increased in high-cycle fatigue zone (Fig. 5).

The fatigue crack incubation factor (A) is obtained by a ratio of the specified number of cycles to the number of cycles prior to a fatigue initiation. That is, $A_i = n_i / N_{al}$, where n_i is the number of occurrences of cycles of type i over the life t of the

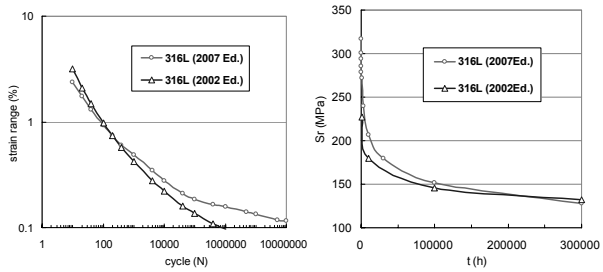

(a) Fatigue strength (b) Creep rupture strength

Fig. 5. Change of material properties in the RCC-MR A3 (10).

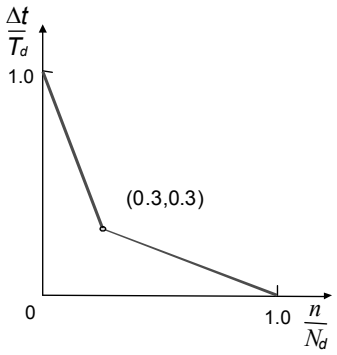

Fig. 6. Creep-fatigue interaction diagram.

component under investigation, and N_{al} is number of cycles prior to initiation of cycle type i, determined from the fatigue curves provided in A3 for the maximum temperature during the cycle.

The creep crack incubation factor (W_i) is obtained by a ratio of the specified duration of a hold time, Δt, to the time prior to a creep initiation, T, determined from the resultant creep rupture property. The sustained stress during the hold time is determined at the distance, d, from the defect, and the usage fraction to creep rupture is calculated. The total usage fraction for initiation, A, and the creep usage fraction for total rupture, W, between time *0* and t are calculated on the basis of a linear sum for all specified cycles. These are expressed as $A=\sum A_i$ and $W=\sum W_i$.

If a calculated point for the incubation factors reaches the creep-fatigue interaction envelope shown in Fig. 6, it means that the crack initiation has occurred due to the creep-fatigue loads under investigation.

The evaluation results of the C-F CI according to A16 for the defect in Fig. 2 are given by Eqs. (3), (4), and (5) for the mechanical loads of 30, 40, and 50 tons, respectively. In this assessment, a stress relaxation was taken into account.

$$\frac{n}{3291}+\frac{\Delta t}{4073}\le D \tag{3}$$

$$\frac{n}{1682}+\frac{\Delta t}{2340}\le D \tag{4}$$

$$\frac{n}{839}+\frac{\Delta t}{1487}\le D \tag{5}$$

When the 2002 edition was used, the C-F CI was evaluated as in Eqs. (6), (7), and (8) for the mechanical loads of 30, 40, and 50 tons, respectively. The results mean that creep crack incubation occurs as soon as the loads are applied.

$$\frac{n}{1610}+\frac{\Delta t}{\to 0}\le D \tag{6}$$

$$\frac{n}{953}+\frac{\Delta t}{\to 0}\le D \tag{7}$$

$$\frac{n}{611}+\frac{\Delta t}{\to 0}\le D \tag{8}$$

When the two sets of the results are compared, it is shown that the 2007 edition gives less conservative results for the fatigue damage than the 2002 edition, while it is significantly less conservative for creep damage.

Since the strain ranges were from 0.445% (30 tons) to 0.622% (50 tons), where the fatigue strength of the 2007 edition was higher than that of the 2002 edition, as shown in Fig. 5(a), the fatigue lifetimes for the 2007 edition were calculated as higher than that of the 2002 edition, as shown in Eqs. (1-3).

The creep rupture strengths (CRS) ranged from 200-250 MPa, where CRS data for the 2007 edition is higher than that of the 2002 edition, as shown in Fig. 5(b). Therefore, the creep rupture times according to the 2007 edition were determined to be much less conservative than that of the 2002 edition, as shown in Eqs. (1-3).

2.3 Assessment of the creep-fatigue crack growth

In the A16 guide, the amount of C-F CG is determined by linearly adding the FCG (Fatigue Crack Growth) and CCG (Cree Crack Growth). The guidelines of design evaluation or defect assessment for high-temperature components as well as low-temperature components operating below creep regime usually adopt a linear elastic approach with the introduction of various coefficients or factors. These can take the inelastic behavior of the component into account in order to come up with consistent and easy reproduction of the results.

The CCG rate is derived from a C^*-integral, based on the reference stress concept and the da/dt- C^* material curve. The formulae on crack growth in the 2007 edition of the A16 have been changed from the 2002 edition (Table 1), which may have a significant effect on crack growth behavior. The major changes in the determination procedures of the reference stresses are shown in Fig. 7.

2.3.1 Calculation of the FCG (δa_f)

The maximum effective stress intensity factor (SIF) range can be calculated from the updated size of the defect due to a fatigue load. The fatigue crack growth is estimated from the Paris law with an SIF range of ΔK_{eff}, as shown in Eq. (9).

$$\Delta K_{eff}=q\sqrt{E^*\Delta J} \tag{9}$$

where q is the closure (R <0) and mean stress (R>0) coeffi-

Table 1. Change in fracture parameter formulae in A16.

A16 (2007)	A16 (2002)
$J_{S,A}=\left(\sqrt{J_{el}^{me}}+k_{th1}^{*}\cdot\sqrt{J_{el}^{th}}\right)^2$ $J_{S,B}=\left(\sqrt{J_{el}^{me}}+k_{th2}^{*}\cdot\sqrt{J_{el}^{th}}\right)^2$	$J_{S,A}=\left(\sqrt{J_{el}^{me}}+k_{th}^{*}\cdot\sqrt{J_{el}^{th}}\right)^2$ $J_{S,B}=\left(\sqrt{J_{el}^{me}}+\frac{\sigma^{me+th}}{\sigma_{el}^{me+th}}\cdot\sqrt{J_{el}^{th}}\right)^2 \cdot\frac{E\cdot\varepsilon_{ref}^{me+th}}{\sigma_{ref}^{me+th}}$
$C_S^{*}=\left(\sqrt{C_S^{me}}+\kappa_{C^*}\cdot k_{C^*th}\cdot\sqrt{J_{el}^{th}}\right)^2$	$C^{*}=\left(\sqrt{J_{el}^{me}}+\frac{\sigma^{me+th}(t)}{\sigma_{el}^{me+th}}\cdot\sqrt{J_{el}^{th}}\right)^2 \cdot\frac{E\cdot\dot{\varepsilon}_{ref}^{me+th}(t)}{\sigma_{ref}^{me+th}(t)}$

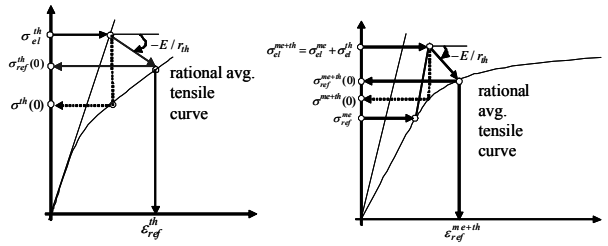

(a) 2007 edition (b) 2002 edition

Fig. 7. Reference stress and strain in A16 guide.

cient, E^* is E for the plane stress and $E/(1-\nu^2)$ for the plane strain, and R is the minimum to maximum load ratio.

In the A16 guide, the SIF K_I for a circumferential defect of cylindrical structure is given by Eq. (10) using an influence function method.

$$K_I=\left(\sigma_m F_m+\sigma_b F_b+\sigma_{gb}F_{gb}\right)\sqrt{\pi c} \tag{10}$$

where σ_m, σ_b , and σ_{gb} are the membrane bending, and global bending stresses, respectively. F_m, F_b , and F_{gb} are the influence coefficients, and 2c is the length of the defect.

The J-integral in the current A16 guide under a combined mechanical loading and a thermal gradient is

$$J_s=\left(\sqrt{J_{el}^{me}}+k_{th}^{*}\cdot\sqrt{J_{el}^{th}}\right)^2 \tag{11}$$

where $J_{el}^{me}=\frac{\left(K_{eq}^{me}\right)^2}{E^*}, J_{el}^{th}=\frac{\left(K_{eq}^{th}\right)^2}{E^*}$; the plane strain is $E^*=E/(1-\nu^2)$, the plane stress is $E^*=E$, and the coefficient providing two options in the calculation of J_s is k_{th}^{*}. The increment of a fatigue propagation for each cycle type i is then calculated from Eq. (12),

$$\left(\delta a_f\right)_i=C\cdot\left[\left(\Delta K_{eff}\right)_i\right]^n \tag{12}$$

where $\left(\Delta K_{eff}\right)_i$ is the effective SIF range for cycle type i. From Eq. (12), the fatigue crack growth rates for options a and b under a mechanical load of 30 tons are calculated in Eqs. (13) and (14), respectively.

$$\left.\frac{da}{dN_f}\right|_a=0.000123\ [mm/cycle] \tag{13}$$

$$\left.\frac{da}{dN_f}\right|_b=0.000582\ [mm/cycle] \tag{14}$$

2.3.2 Calculation of the CCG (δa_c)

For the calculation of a CCG, the fracture parameter of C^*-integral should be determined during the hold time. The amount of a CCG during the given hold time t_{mi} is calculated from Eqs. (15) and (16). It should be noted that the formula for the 2002 edition shown in Eq. (16) is quite different from Eq. (15) of the 2007 edition.

$$C_s^{*}=\left(\sqrt{C_s^{me}}+\kappa_{C^*}\cdot k_{C^*th}\cdot\sqrt{J_{el}^{th}}\right)^2 \tag{15}$$

$$C^{*}=\left(\sqrt{J_{el}^{me}}+\frac{\sigma^{me+th}(t)}{\sigma_{el}^{me+th}}\cdot\sqrt{J_{el}^{th}}\right)^2\cdot\frac{E\cdot\dot{\varepsilon}_{ref}^{me+th}(t)}{\sigma_{ref}^{me+th}(t)} \tag{16}$$

$$\left(\delta a_c\right)_i=\int_{t_i}^{t_i+t_{mi}}A\left[C_i^{*}(t)\right]^q\mathrm{d}t \tag{17}$$

where C_s^{me} is the C^* integral for the mechanical loads, J_{el}^{th} is the J-integral under the thermal loads, and $C_i^{*}(t)$ is the C^* integral at time t. κ_{C^*} is the interaction coefficient for the influence of mechanical loading on the elasto-plastic correction for thermal loadings. A pessimistic value of $\kappa_{C^*}=1.6$ is provided, and another value can be used if it can be justified. In addition, κ_{C^*th} is elasto-plastic correction for thermal loadings.

Eqs. (15) and (16) are used for the assessment of CCG. When the primary creep law is applied to determine the thermal C^* integral, $C_s^{*}=0.001$, 0.050, and 0.102 *N/mm·hr* for mechanical loads of 30, 40, and 50 tons, respectively. On the other hand, when the secondary creep law is applied, $C_s^{*}=0.689$, 1.101, and 1.620 *N/mm·hr* for mechanical loads of 30, 40, and 50 tons, respectively.

Calculations of the C-F CG can be carried out for combinations of creep options (primary or secondary) and fatigue options (option a or b). The calculated results for the four cases are shown in Fig. 8, where 'primary creep with Option B' is the upper bound and 'secondary creep with Option A' is the lower bound under the mechanical load of 30 tons.

The images of the upper and lower bounds for the two editions are shown in Fig. 9 when the actual loading of Fig. 3(b) is applied. It is shown that the 2007 edition gives a wider range of the C-F CG than the 2002 edition.

It should be noted that since the reference mechanical stress used to determine the C^* integral in the present problem is low [10], the actual 316L steel should be at a primary creep condition. Therefore, the lower bound case of 'secondary creep with

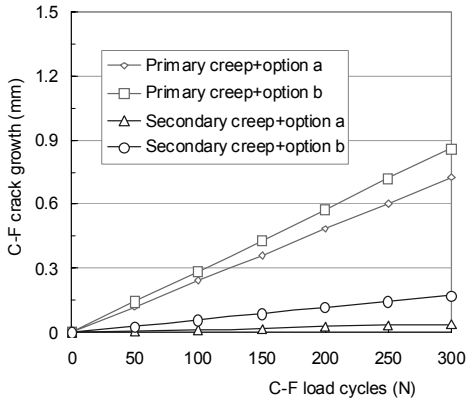

Fig. 8. Comparison of creep-fatigue crack growth under mechanical loads of 30 tons.

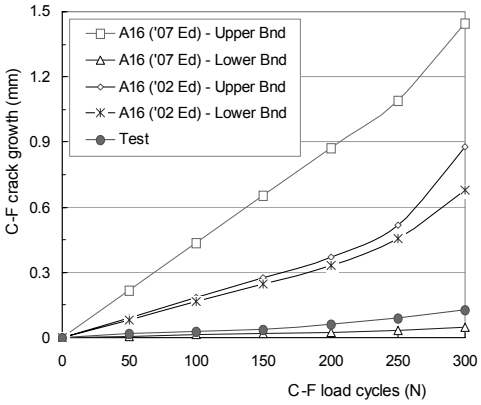

Fig. 9. Comparison of the results on creep-fatigue crack growth.

option A' in Fig. 8 is not physically valid in the present test condition, but this is the calculation on the lower bound for the reference. In the case that the secondary creep is considered, the 2007 edition gives lower values of crack growth than that of the 2002 edition (Fig. 9).

3. Comparison of the results by the structural test and assessment

3.1 Structural specimen

The structural specimen in Fig. 1 had several circumferential weld lines in outer shell. One through-wall defect with a length of 14 mm was machined by an electrical discharge machining at the 316L part of the specimen, as shown in Fig. 1(b). The schematic diagram of the specimen set-up is shown in Fig. 10. The loads of Fig. 3 were applied to the specimen.

There were several circumferential weld lines on the outer shell of the specimen shown in Fig. 2. Weld residual stresses were induced on the specimen during the fabrication process [19, 20]. However, it was shown that the residual stresses relaxed rapidly in high-temperature structures. The residual stresses at high temperatures are known to contribute to crack initiation at the initial stage of the loading; however, they do not contribute to crack growth [21].

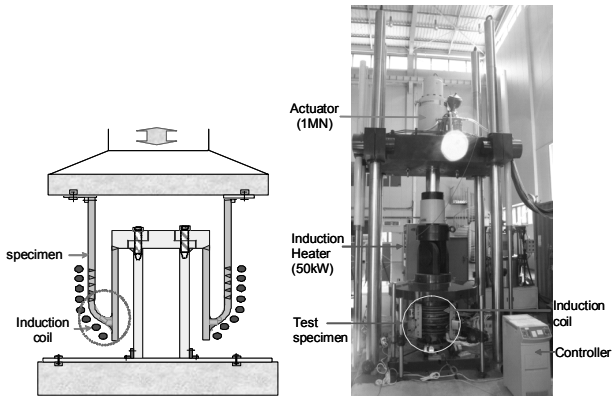

(a) (b)

Fig. 10. Creep-fatigue test facility.

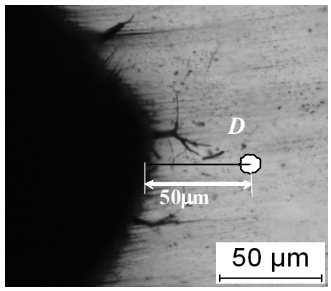

Fig. 11. Observed image on creep-fatigue crack initiation (N=50 cycles).

Three hundred creep-fatigue load cycles were applied to the present specimen, and the images of the specimen surfaces were obtained. A portable optical microscope was used to observe the creep-fatigue crack behavior of the test specimen with an interval of 50 cycles (hold time=100 h) up to 300 cycles.

3.2 Observed image on crack initiation and comparison with assessment results

The image of Fig. 11 shows that no distinct crack initiation up to the *D* point 50 μm ahead of the tip occurred until 50 creep-fatigue load cycles were applied. Observation was carried out at the defect machined at the 316L stainless steel part, as shown in Fig. 1(b). This observed image can be compared with those of the assessments described in Section 2.2.

Under a mechanical loading of 30 tons, the assessment result on C-F CI was calculated from Eq. (3) when the 2002 edition of the A16 was followed, and calculated from Eq. (6) when the 2007 edition was followed. Calculated according to the 2002 edition, Eq. (6) means that C-F CI occurs as soon as loading is applied because of the high creep damage, which is apparently overly conservative for the present problem. In the meantime, Eq. (3) calculated according to the 2007 edition shows C-F CI occurs far later than that of the 2002 edition because the fatigue lifetime is 3291 cycles and the creep rup-

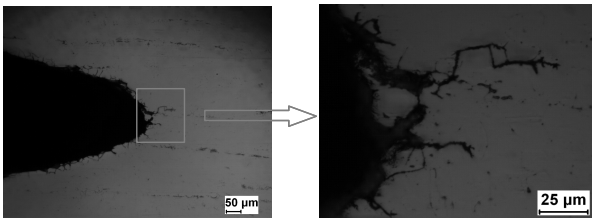

Fig. 12. Observed image on creep-fatigue crack growth (N=300 cycles).

ture time is 4073 h. From the above comparison, it was shown that the A16 guide of the 2007 edition is less conservative than that of the 2002 edition in terms of C-F CI.

The assessment procedure of A16 on C-F CI has not been revised, but the material properties in the A3 [10] have been changed. It was shown that the reduction of the conservatism on C-F CI is caused mainly by the change of the creep rupture strength as well as fatigue strength data in the A3.

3.3 Observed image on crack growth and comparison with assessment results

The observed images of crack growth after 300 creep-fatigue load cycles show that surface crack has occurred, as shown in Fig. 12. The progressive crack growth aspects at every 50 load cycles are shown in Fig. 9. When the images are compared with the assessment results of Fig. 9, the overall trends of the assessments in both editions are conservative, except in the lower bound of the 2007 edition. The lower bound is the combination of 'Option A' in the evaluation of FCG and 'secondary creep' in the evaluation of stress relaxation regarding the formula of C^*-integral. Since the actual creep-fatigue loading condition is obviously a primary creep-dominant creep condition, the present case study with a secondary creep is not a practical assumption; therefore, it is not surprising that the assessment results on C-F CG are higher than those of the test.

From another point of view, it should be noted that when the secondary creep was used for the two editions, the 2007 edition gives a lower amount of C-F CG than the 2002 edition, which could lead to a more conservative C-F CG for a loading dominated by a secondary creep.

4. Conclusions

An assessment on C-F CI and C-F CG for a 316L stainless steel structure was carried out according to the French assessment procedure of RCC-MR A16. The results were compared with those of the structural tests. In this study, the A16 procedures of the 2007 edition and the 2002 edition were used, and quantification on the changes of the procedures (A16) and material properties (A3) between the two editions in terms of C-F CI and C-F CG was carried out. Modifications in the A3 affected the results on the assessments of C-F CI and C-F CG, whereas modifications of the A16 affected only C-F CG because no change has been made in the assessment guideline on C-F CI.

As for the assessment of C-F CI, the change of the creep rupture strength as well as fatigue strength data was shown to significantly affect the results. When the assessment results on C-F CI from the 2007 edition, the 2002 edition, and the observed images were compared, it was found that the results by the 2002 edition were overly conservative while that by the 2007 edition were reasonable. Therefore, it was shown that the assessment results on C-FCI according to the 2007 edition were less conservative with the modified A3 properties than the 2002 edition.

As for the assessment on C-F CG, the formulae on FCG and CCG in the A16 have been changed in addition to the changes of the A3. Since the present creep-fatigue loading was a dominant-primary creep condition, the assessment results by the 2007 edition were shown to be more conservative.

When the observed images were compared with the assessment results, the overall trends of the assessments in both editions were conservative. The 2002 edition was more conservative for the assessment of C-F CI, while the 2007 edition was more conservative for the assessment of C-F CG under the dominant primary creep loading conditions.

Acknowledgements

This study was supported by the Korean Ministry of Education, Science, and Technology through its National Nuclear Technology Program.

References

[1] D.-H. Hahn et al., KALIMER-600 Conceptual Design Report, KAERI/TR-3381, Korea Atomic Energy Research Institute, Daejeon, (2007).
[2] ASME Boiler and Pressure Vessel Code, Section III, Rules for Construction of Nuclear Power Plant Components, Div. 1, Subsection NH, Class 1 Components in Elevated Temperature Service, ASME, (2007).
[3] RCC-MR, Section I Subsection B, Design and Construction Rules for Mechanical Components of Nuclear Installations, 2007 Edition, AFCEN, (2007).
[4] High temperature structural design guideline for fast breeder demonstration reactor (draft), JAPC (1999).
[5] RCC-MR, Section I Subsection Z, Technical Appendix 16, Design and Construction Rules for Mechanical Components of Nuclear Installations, 2007 Edition, AFCEN, (2007).
[6] R5, Assessment procedure for the high temperature response of structures, Issue 3, British Energy Generation Ltd, (2003).
[7] BS7910, Guide on methods for assessing the acceptability of flaws in metallic structures, British Standards, (1999).
[8] API579, API Recommended Practice 579, API, (2001).
[9] FITNET FITNESS-FOR-SERVICE Procedure, Rev. MK8, ISBN 978-3-940923-00-4, (2008).
[10] RCC-MR, Section I Subsection Z Technical Appendix A3, Design and Construction Rules for Mechanical Components of Nuclear Installations, (2007).

[11] H.-Y. Lee, J.-H. Lee and B.-H. Kim, Creep-fatigue crack growth behavior of a structure with crack like defects at the welds, *Journal of Mechanical Science and Technology*, 20 (12) (2006) 2067-2076.

[12] H.-Y. Lee, J.-B. Kim, S.-H. Kim and J.-H. Lee, Assessment of Creep-Fatigue Crack Initiation for Welded Cylindrical Structure of Austenitic Stainless Steels, *International Journal of Pressure Vessel and Piping*, 83 (2006) 826-834,.

[13] Ph. Metheron. and S. Chapuliot, Fatigue initiation of crack under mode III and mixed mode I+III Loads in a 9Cr steel, *18th Int. Conf. on SMIRT*, Beijing, China, pp. 1896-1903, August, p.7, (2005).

[14] O. Ancelet and S. Chapuliot, Mechanical behavior of HTR materials : developments in support of defect assessment, structural integrity and lifetime evaluation, *Proceedings of ICAPP 2007,* Nice, France, May 13-18 (2007) Paper 7182.

[15] H.-Y. Lee, J.-H. Lee and K. M. Nikbin, Assessment of High Temperature Crack Behaviour for a Structure with Defects, *Journal of Pressure Vessel Technology, Transactions of ASME*, 131 (2010) 031403-1~7.

[16] H.-Y. Lee, J.-B. Kim, W.-G. Kim and J.-H. Lee, Creep-fatigue Crack Behaviour of a Mod 9Cr-1Mo steel structure with weldments, *The Transactions of the Indian Institute of Metals*, in press (2010).

[17] H.-Y. Lee, S.-H. Lee, J.-B. Kim and J.-H. Lee, Creep-fatigue damage for a structure with dissimilar metal welds of Mod 9Cr-1Mo and 316L stainless steel, *International Journal of Fatigue*, 29 (2007) 1868-1879.

[18] ABAQUS Users manual, Version 6.7, H.K.S, USA, (2007).

[19] H.-Y. Lee, J.-B. Kim, J.-H. Lee and K. M. Nikbin, Comprehensive Residual Stress Distribution for a Plate and Pipe Components, *Journal of Mechanical Science and Technology*, 20 (3) (2006) 335-344.

[20] H.-Y. Lee, F. Biglari, R. Wimpory, N. P. O'Dowd, and K, M. Nikbin, Treatment of residual stresses in life assessment procedures," *Engineering Fracture Mechanics*, 73 (2006) 1755-1771 (2006).

[21] H.-Y Lee and K. M. Nikbin, Modelling the Redistribution of Residual Stresses at Elevated Temperature in Components, *Journal of ASTM International*, 3 (1) (2006) 111-125.

Hyeong-Yeon Lee, Ph.D at KAIST (Korea Advanced Institute of Science and Technology) at Dept. of Aerospace Engineering in 1995. Principal researcher at Korea Atomic Energy Research Institute Specialty is design and assessment of high temperature structures, Assessment of creep-fatigue interaction, crack behavior at elevated temperature.